Chem. Chem. Technol., 2025,
Vol. 20, No. 1, pp. 010–027

Chemistry

SUSTAINABLE VALORISATION OF FLY ASH INTO GEOPOLYMER-BASED ADSORBENT: STRUCTURAL OPTIMIZATION AND METHYLENE-BLUE REMOVAL PERFORMANCE

Khoa Dang Nguyen[1,✉], Anh Thi Kim Phan[1], Anh Phuong Le Thi[2], Sujitra Onutai[3], Ky Ngoc Hoa Nguyen[4]

[1] Faculty of Environment, Van Lang School of Technology, Van Lang University, Binh Loi Trung Ward, Ho Chi Minh City 70000, Vietnam
[2] Research Center for Negative Emissions Technologies, Kyushu University, 744 Motooka, Nishi-ku, Fukuoka 819-0395, Japan
[3] Key Laboratory of Advanced Materials of Tropical Island Resources of Ministry of Education, School of Materials Science and Engineering, Hainan University, Hainan, 570228, PR China
[4] Faculty of Basic Sciences, University of Phan Thiet, Lam Dong Province, 77100, Vietnam
✉ *khoa.nd@vlu.edu.vn*

https://doi.org 10.23939/chcht20.01.010

Abstract. In this study, fly ash (FA)-based geopolymers were synthesized using varying proportions of sodium silicate/sodium hydroxide (Na_2SiO_3/ NaOH 10M) solution, ranging from 49% in the 51FA sample to 67% in the 33FA sample, used for the adsorption of methylene blue (MB) in water. Following curing at 60°C for 24 h, the porosity of the resulting geopolymers decreased, attributed to the enhanced polycondensation process driven by the increased Na_2SiO_3 content, which resulted in the formation of a more compact gel structure in the obtained geopolymer. The Weber–Morris model indicated that surface interactions with MB molecules were predominant in the 51FA sample, while pore-filling mechanisms were more pronounced in the 33FA geopolymer. Adsorption experiments revealed that all geopolymer samples conformed to the Langmuir isotherm model, with correlation coefficients approaching unity.

Keywords: alkali activator, binder, geopolymer, fly-ash, regenerated waste

1. Introduction

Coal-fired power plants are significant contributors to air pollution, with fly ash, a by-product of combustion-posing substantial environmental and economic challenges. The associated health risks for humans lead to increased healthcare costs and reduced productivity due to illness. The integration of fly ash into geopolymers presents a promising solution, transforming waste materials into valuable construction products, which promote both environmental sustainability and economic benefits. Currently, over 20 coal-fired power plants in Vietnam generate approximately 15.7 million tons of fly ash annually. By 2025, Vietnam aims to expand coal-fired power capacity from 33% to 55%. It is projected that by 2030, 46 new coal-fired thermal power plants will be operational, with current fly ash production estimated at approximately 25 million tons per year.[1] However, only 30% of the total fly ash can be recycled into useful products. The unrecycled fly ash is typically accumulated, which poses serious ecological risks and heightens the potential for natural disasters. Groundwater sources may be contaminated if they encounter fly ash storage areas, leading to changes in sediment pH and permeability, clogging groundwater channels, and rendering the water turbid and unfit for use. Additionally, as fly ash accumulates, its toxins are released into the atmosphere, further polluting the air around the disposal sites.[2] The reuse of coal fly ash within the framework of a circular economy is increasingly recognized as a key strategy for reducing waste and recovering valuable materials. As a byproduct of coal combustion, coal fly ash has traditionally been viewed as an environmental challenge, but its potential for sustainable reuse is significant. It is now being utilized in the production of eco-friendly building materials, such as concrete, which helps to lower the environmental impact of construction while reclaiming useful minerals like alumina and silica. Recent research has introduced innovative methods for extracting valuable components from coal fly ash, including alumina, through techniques such as vacuum thermal reduction, hydrochemical processing, and alkali dissolution. These

processes not only reduce waste but also improve resource efficiency by converting a problematic byproduct into a valuable resource.[3] This approach not only reduces waste but also enhances resource recovery, contributing to a more sustainable and efficient use of materials within the industrial sector.[4]

Geopolymers are indeed an innovative class of inorganic polymers formed through the reaction of alumina-silicate oxides with alkali metal silicate solutions under highly alkaline conditions.[5,6] Their unique three-dimensional network structures, which can vary based on the Si/Al ratio, play a crucial role in determining their mechanical properties. The different structures, such as polysialate (–O–Si–O–Al–O–), polysialate siloxo (–O–Si–O–Al–O–Si–O–), and polysialate disiloxo (O–Si–O–Al–O–Si–O–Si–O–), are influenced by the initial Si/Al ratio in the raw materials, which typically ranges from 3.0 to 3.8.[7] Research has shown that the choice of starting materials rich in SiO_2 and Al_2O_3 is essential for effective geopolymerization.[8,9] The activation process often involves high-concentration alkali solutions, such as NaOH or KOH, along with sodium silicate as a binder (Na_2SiO_3).[10] Notably, geopolymers activated with NaOH tend to exhibit superior compressive strength compared to those activated with KOH at equivalent concentrations.[11] The recommended concentration of the alkali solution generally falls between 5 to 15 M, with 10 M being optimal for achieving desirable mechanical properties.[7,12] Temperature also plays a significant role in the geopolymerization process. Curing temperatures between 60°C and 80°C are ideal, as higher temperatures can compromise the structural integrity of the geopolymer.[13] Additionally, the effect of mixing ratio of Na_2SiO_3/NaOH in the preparation of geopolymer was studied,[14] which was typically around 2.5, which aids in enhancing the silica content and promoting the formation of Si–O–Si linkages, thus contributing to the overall strength of the geopolymer.[7] Most studies have concentrated on the use of coal fly ash as a primary raw material for geopolymers, highlighting its potential for sustainable construction materials and applications in wastewater treatment through adsorption processes. Therefore, fly-ash-based geopolymer is a promising material for both environmental and engineering applications.[9] However, the portion of this mixture was not well studied in terms of different amounts in the geopolymer composition. Hence, we aimed to prepare FA-based geopolymer with various amounts of Na_2SiO_3 in the activator mixture in the presence of NaOH solution.

Globally, dye pollution from the textile industry is a significant environmental challenge, contributing to water contamination and posing risks to ecosystems and human health. The textile sector releases large quantities of wastewater containing hazardous chemicals, including synthetic dyes like azo compounds, which are difficult to remove using conventional treatment methods. These chemicals can harm aquatic life, degrade water quality, and negatively impact the environment. It is estimated that nearly half of dyes are discharged into the environment as pollutants, primarily due to the weak interaction between fibers and dyes.[15] These dyes exhibit a propensity to bind with other compounds, possess a slow biodegradation rate, and exhibit high chromatic intensity.[16] The elevated concentration of inorganic dyes in the environment adversely affects ecosystem quality by obstructing sunlight penetration and disrupting biological processes in aquatic systems.[17] Furthermore, these dyes are highly toxic and can significantly alter the landscape of the affected areas. Methylene blue (MB) is a synthetic dye that is widely used in industries such as textiles, printing, and pharmaceuticals.[18] However, its presence in water bodies due to industrial discharge poses a significant environmental problem. The dye is known for being highly visible, even at low concentrations, and it is resistant to natural degradation, making it persistent in aquatic environments.[19] One method that has garnered considerable attention for its simplicity, environmental sustainability, cost-effectiveness, and potential efficiency is adsorption.[20] The objective of this study is to identify suitable adsorption materials as geopolymer regenerated from industrial waste, such as coal fly ash, for the effective removal of MB from wastewater.

2. Experimental

2.1. Materials

The fly ash (FA) generated from coal combustion in this study was collected from the Le Minh Xuan Industrial Zone, Ho Chi Minh City (Fig. 1a). The samples were ground and sieved using a 245-μm sieve, then dried at 105°C for 24 h. The main chemical composition, determined through X-ray fluorescence (XRF), included SiO_2 35.2%, Al_2O_3 25.9%, CaO 7.6% and Na_2O 1.5%. Fig. 1b displayed a scanning electron microscope (SEM) micrograph of the FA at 3000× magnification. The FA contained various spherical particles with an average diameter of 50 μm. Additionally, impurities were observed in Fig. 1c at 3000× magnification. Hydrochloric acid (HCl, 36%), sodium hydroxide (NaOH, 99%), sodium silicate (Na_2SiO_3, with SiO_2 content of 28.5%, and Na_2O content of 8.5%), and methylene blue (MB) were sourced from Merck, Germany. All chemicals used in the preparation of the geopolymer and the MB-adsorption experiment were of analytical grade.

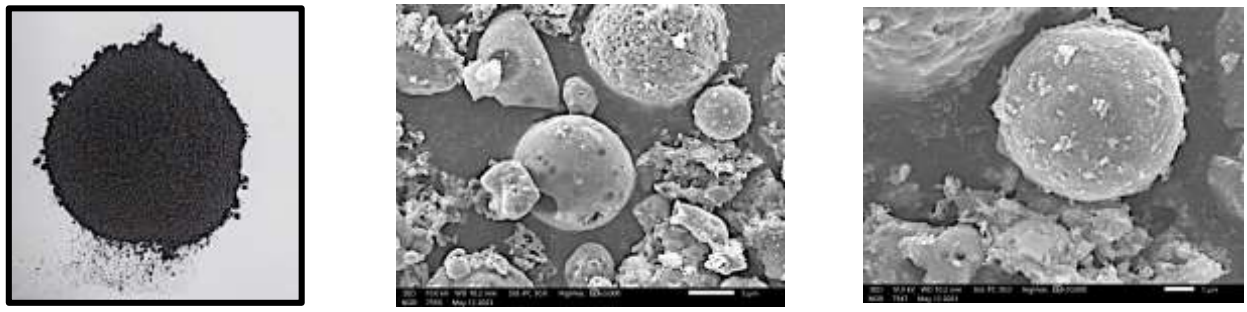

a b c

Fig. 1. Appearance of FA a), SEM image of FA at magnification of 500× b) and 3000× c)

2.2. Methods

2.2.1. The preparation of geopolymer from fly ash

The pretreated FA was mixed with the appropriate amount in addition to NaOH and Na_2SiO_3 aqueous solution. The ratio between Na_2SiO_3/NaOH was kept at 2.5. The loading of FA was varied in the range of 33 to 51%, noted as 51FA, 42FA, and 33FA (Table 1). The paste was mixed within 5 min at room temperature before pouring into the silicon mold ($20 \times 20 \times 20\, mm^3$) followed by drying at 60°C for 24 h. After that, geopolymers were obtained as seen in Fig. 2. Before measurements, these samples were ground and sieved through a 245µm-mesh sieve and washed in an excess amount of deionized water until the pH reached a neutral value.

2.2.2. Characterization of the obtained geopolymer

The surface morphologies of the samples were examined using a scanning electron microscope (SEM) (JSM-IT300, JEOL, Japan). Prior to imaging, the samples were coated with a thin layer of conductive material (gold) to enhance electron conductivity. Imaging was performed at various magnifications under an accelerating voltage ranging from 10 to 15 kV. Furthermore, to analyze the elemental distributions within the synthesized geopolymers, an energy-dispersive spectrometer (EDX) (JSM-5300LV, JEOL Ltd., Japan) was integrated with the SEM system.

The transformation of the raw material into geopolymer after alkali solution activation was evaluated using Fourier Transform Infrared Spectroscopy (FT-IR) (Microscope LUMOS, Bruker, Germany). The dried samples were ground with potassium bromide (KBr) for measurement in ϕ transmittance mode. The spectra were recorded in the wavenumber range of 4000 – 400 cm^{-1} with a resolution of 2 cm^{-1}. Additionally, the geopolymer after methylene blue (MB) adsorption was analyzed to observe spectral differences. In addition, the deconvolution of the IR spectra in the range of 1300 – 800 cm^{-1} was carried out. The centers of the fixed peaks obtained from the spectral data were decomposed into their Gaussian components. The peal centers and the curve were then fitted using OriginPro 8.5.

The Brunauer-Emmett-Teller (BET) surface area and pore size distribution of the geopolymer samples were measured using a Tristar II surface area and porosity analyzer (Shimadzu). The geopolymer powders were dried under vacuum conditions for 24 hours before nitrogen gas adsorption at 77 K.

Table 1. Mixing portion of the geopolymer prepared from fly ash for 100 g

No.	Sample	FA (wt%)	Na_2SiO_3 (wt%)	NaOH 10 M (wt%)	Na_2SiO_3/NaOH
1	51FA	51	35	14	2.5
2	42FA	42	41.4	16.6	
3	33FA	33	47.9	19.2	

The pH point of zero charge (pH_{pzc}) was determined to assess the adsorption performance of geopolymers in relation to solution pH. Approximately 0.05 g of geopolymer was placed in glass Erlenmeyer flasks containing 20 mL of 0.1M NaCl aqueous solution. The initial pH (pH_i) was adjusted to 2, 4, 6, 8, 10, and 12 using 1N NaOH and 1N HCl solutions. The samples were agitated for 180 min at 300 rpm at 27°C. The final pH (pH_f) of the solution was measured for each sample, and the pH_{pzc} values were calculated when the change in pH (ΔpH) was zero.

2.2.3. The adsorption experiment of methylene blue

Stock MB solutions of 1000 mg/L were prepared by dissolving in deionized water. The working solution was diluted to the desired concentration. The adsorption of MB to geopolymer samples was measured by the following process. Approximately 0.1 g of the dry powder of geopolymer as an adsorbent was immersed directly into glass flasks containing 20 mL of initial solutions of 100 $mg{\cdot}L^{-1}$. The pH of the MB solutions adjusted with 1M NaOH aqueous solution was from 2 to 12. After 3 h of agitation at 200 rpm at 300 K, the samples were centrifuged at 8000 rpm for 15 min to remove the adsorbed powders. After that, the remaining concentration of MB in the centrifuged solution was determined by UV–Vis spectrometry (PG Instrument, T60) at a wavenumber of 664 nm.

Here, the removal percentage (H %) (Eq. 1) was:

$$\text{H (\%)} = \frac{C_0 - C_t}{C_0} \times 100 \qquad (1)$$

where H was the removal capacity of the MB absorbed at equilibrium (%); C_o and C_t are the initial MB concentration and the concentrations in time (mg/L), respectively; M is the weight of the absorbents (g); and V is the solution volume (L).

The uptake amounts q_t of MB to the geopolymer were calculated by the following equation (Eq. 2):

$$q_t = \frac{C_0 - C_t}{M} \times V \qquad (2)$$

where q_t was the amount of MB absorbed at the current time (mg/g).

3. Results and Discussion

3.1. The appearance of the geopolymers

Fig. 2 shows the images of the geopolymer samples prepared from FA with different mixing ratios on the lateral face (upper row). It was seen that the geopolymer exhibited uniformity based on the initial mold size (20 × 20 × 20 mm^3). The mixing ratio directly influenced the external appearance of the corresponding materials. Indeed, when the ratio of the activating mixture increased from 49% to 67% during the geopolymer synthesis process, the porous structure of the geopolymers was obtained in higher intensity as seen in 51FA and 33FA. Therefore, it was observed that the material structure was somewhat affected.

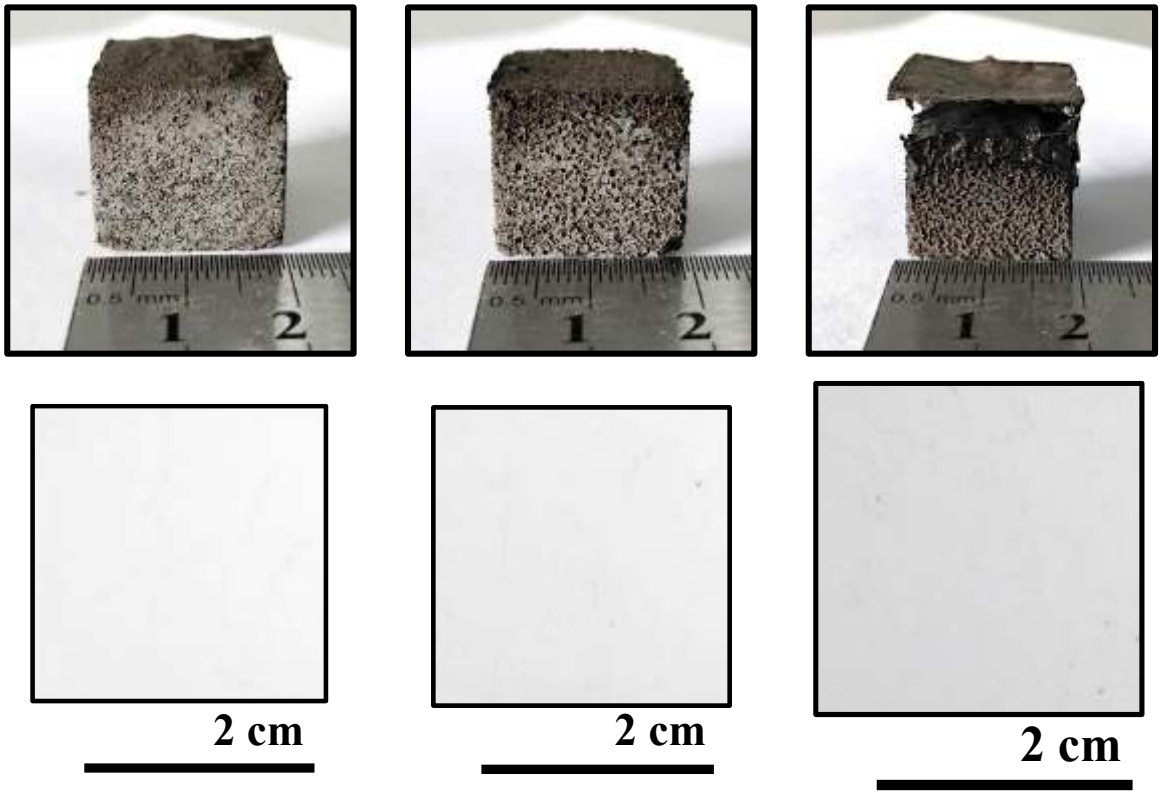

Fig. 2. Images of the prepared geopolymer on the lateral face (first row) and base face (second row) of 51FA a), 42FA b), and 33FA c)

This result could be explained by the increased mass of the activating mixture (Na_2SiO_3/NaOH) and the sample curing process at 60°C, which caused the disruption in the geopolymer structure, leading to a greater release of water molecules. As observed from the base and lateral views of the samples (bottom row), numerous pores developed following the geopolymerization process, which was typically associated with the release of water and the formation of reaction products within the matrix. In particular, the 33FA geopolymer exhibited pronounced surface cracking, suggesting that significant water evaporation occurred during the curing process at 60°C for 24 h, likely leading to internal stress and shrinkage, which ultimately caused the cracks.[21] These findings highlighted the sensitivity of the microstructure to curing conditions. However, it should be noted that these ratios were successfully synthesized and used in subsequent experiments.

From Table 2, the main chemical compositions were listed to compare the difference before and after the geopolymerization. As seen, the fly ash sample did not contain heavy metals. The SiO_2 (%) content differs between the fly ash (FA) sample and the geopolymer after synthesis. The Si/Al ratio of FA is 1.40. After the synthesis process, involving the alkaline mixture and plasticizer, this ratio increases to 1.82 in the 51FA, 1.47 in the 42FA, and 1.42 in the 33FA. As the content of the activating mixture increased, the percentage mass of SiO_2 was higher compared to the original fly ash material; however, there was no significant difference between the 42FA and 33FA samples. The Al_2O_3 (%) content also followed a similar trend. Notably, the 51FA geopolymer showed a higher SiO_2 content, while the Al_2O_3 content decreased compared to the original FA material. This indicated that during the geopolymer preparation, the NaOH 10M solution dissolved some parts of the Al_2O_3, leading to a loss in the 51FA geopolymer. This could be explained by the reduction in the FA content in the initial mixture for the geopolymerization, which decreased the interaction between the components. Furthermore, the addition of SiO_2 was loaded in a solution form, which might lead to unstable durability after the water-washing process. Another noteworthy observation was that the percentage of Na_2O content in the 51FA sample was found to be higher than in the FA and the 42FA and 33FA. This result once again highlighted the importance of the initial mixing ratio in forming the structure of the corresponding geopolymer sample.

Table 2. The properties of the prepared geopolymers

No.	Sample	Main chemical composition (wt%)				Surface area (m^2/g)	Pore size (nm)	Pore volume (cm^3/g)
		SiO_2	Al_2O_3	Fe_2O_3	Na_2O			
1	51FA	41.1	22.6	18.4	3.5	99.8	4.2	0.089
2	42FA	38.2	25.9	18.8	1.5	95.9	4.0	0.086
3	33FA	37.1	26.2	19.5	1.5	89.7	3.8	0.075

3.2. Properties of the geopolymers

3.2.1. Morphology of the geopolymers

Fig. 3 presents the morphology of the geopolymer prepared at various conditions. It was observed that after the addition of activating agents and binders in the geopolymerization process, the surface of the ash particles became rougher, and the particles increased in size compared to the raw FA (2000×). However, at a magnification of 10,000×, several FA particles were still intact. These were unreacted fly ash particles that remained in the mixture after the activation process, indicating that the surface area of the particles might be interfered with. As seen, the surface morphology of the 51FA was more porous compared to the others. In the cases of 41FA and 33FA, impurity substances were observed to accumulate on the surfaces of the synthesized geopolymers. This phenomenon might be attributed to the increased concentration of alkaline activators used during the preparation process, which likely resulted in the formation of the pore in a smaller volume and size within the geopolymer matrix. Despite this, unreacted FA particles were not detected in the 33FA sample. This absence was likely due to the insufficient availability of reactive precursor materials, which limited the progression of the geopolymerization reaction and ensured that most of the FA was fully consumed during the process.

3.2.2. FT-IR spectra

Fig. 4 illustrates the FT-IR spectra of fly ash (FA) and geopolymer samples with the increasing proportions of the activator mixture during synthesis. In general, across all samples, the spectrum in the wavenumber range of 3400 – 3500 cm^{-1} corresponded to the stretching vibrations of O–H bonds in SiO_2, forming silanol groups (Si–OH).

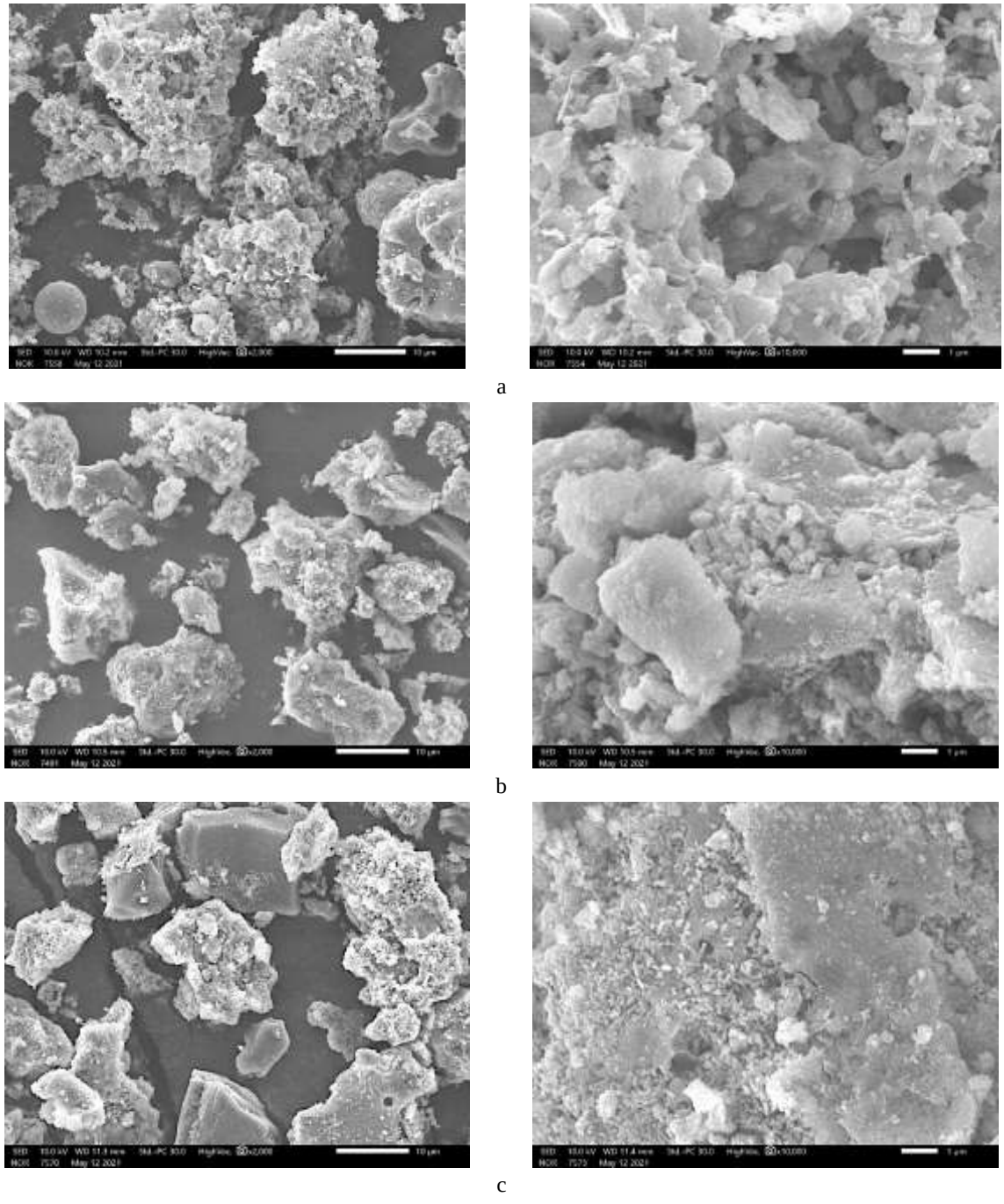

Fig. 3. SEM images of the prepared geopolymer of 51FA a), 42FA b) and 33FA c) at 2000× (left) and 10000× (right)

The intensity of this peak increased as the FA content in the geopolymer samples was enhanced.[22] The wavenumber around 1650 cm^{-1} was assigned to the H–O–H bond, indicating the presence of water molecules intercalated within the material's structure. This suggested that the material exhibits hygroscopic properties under normal conditions.[23] In the case of FA, the spectrum at 788 cm^{-1} was the Al–O bond within the structure of Al_2O_3. Meanwhile, the spectrum at 1102 cm^{-1} indicated the asymmetric stretching vibrations of Si–O–Si bonds.[7] Notably, the wavenumber at 1101 cm^{-1}, presenting the Si–O bond in the structure of FA, was shifted to a shorter wavelength (approximately 990 cm^{-1}), representing Al–O–Si bonds. The intensity of this peak increased correspondingly with the FA content. Additionally, the wavenumber at 1456 cm^{-1} represented the C=O bond in the molecular structure of Na_2CO_3. This

phenomenon could be attributed to the use of a large amount of NaOH and Na_2SiO_3 solutions during the preparation of the geopolymer samples.[7,23] Through the FT-IR spectrum, it was observed that the synthesis of geopolymer from FA with different mixing ratios of Na_2SiO_3 and NaOH 10M has occurred.

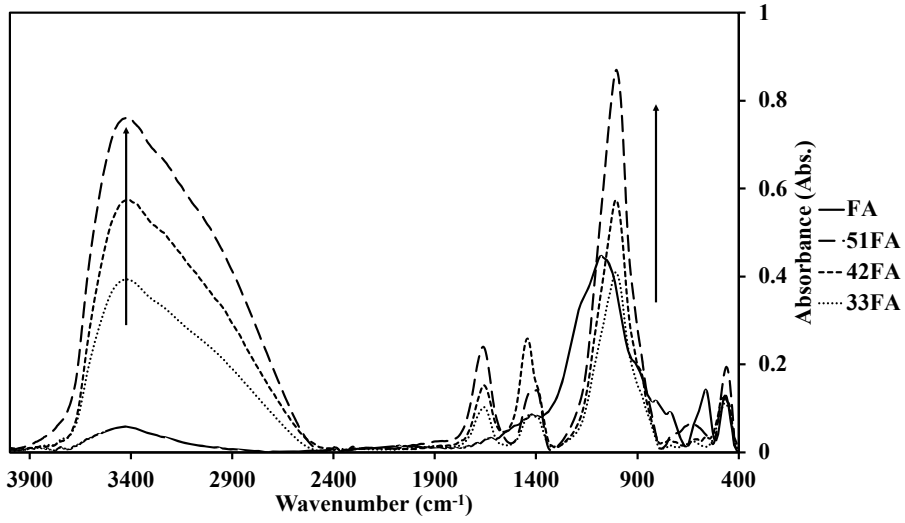

Fig. 4. FT-IR spectra of FA and the prepared geopolymer

To further elucidate the interaction between FA and the activator mixture during the geopolymer synthesis process, the Gaussian differential deconvolution method was applied in the wavenumber range of 1300 – 800 cm^{-1} (Fig. 5). This was used to examine changes in specific bond components corresponding to the various vibrational modes of the geopolymer structures formed, with an excellent fitting correlation (R^2 = 0.9995). Based on reference studies from various authors, five deconvoluted regions representing specific bonds were analyzed in this study. According to H.T.B.M. Petrus *et al.* (2022), peak 1 (1180 – 1110 cm^{-1}) was associated with the asymmetric stretching of Si–O–T bonds in the unreacted fly ash structure. Peak 2 (1095 – 1040 cm^{-1}) represented the stretching of Si–O bonds. Peak 3 (1037 – 997 cm^{-1}) was the T–Si–O bonds in the tetrahedral structure of the geopolymer network. Peak 4 (970 – 920 cm^{-1}) corresponded to the asymmetric stretching of Si–O–Al/Al–O–Si bonds in minerals such as mullite or dickite. Peak 5 (897 – 850 cm^{-1}) is attributed to the bending vibrations of O–H bonds in Si–OH structures from unreacted activator solutions. In Fig. 6a for FA, the peaks 1 and 3 exhibited significant distributions, indicating the presence of the unreacted initial structure. Geopolymer samples with different mixing ratios (Figs. 6b–6d) demonstrated notable differences. The intensity of peak 3 was highest in the 51FA sample and lowest in 33FA. Additionally, peak 4 tended to increase, reflecting an inefficient interaction between FA and the activator mixture. Peak 2 showed a decreasing trend, which was explained by the loss of SiO_2 content during sample washing to neutralize the conditions for subsequent experiments.[24]

The difference in the reaction behaviour of Si–O bonds in sodium silicate and fly ash when exposed to highly concentrated NaOH primarily stemmed from their distinct structural characteristics and reactivity. Sodium silicate was recognized as an amorphous and highly soluble material, existing in glassy or liquid forms, and contained readily available Si–O–Na and Si–O–Si bonds. Upon exposure to concentrated NaOH, these Si–O–Si bonds underwent further depolymerization, resulting in the formation of soluble silicate species such as SiO_4^{4-}, $HSiO_3^-$, and H_2SiO_3.[25] This reaction occurred rapidly due to the high solubility and availability of reactive Si–O bonds.[26] In contrast, fly ash comprised a complex mixture of amorphous and crystalline phases, with Si–O–Si and Si–O–Al bonds forming a three-dimensional network, rendering it less reactive. Hence, NaOH initially attacked the amorphous phase, gradually breaking Si–O and Al–O bonds, leading to the dissolution of silica and alumina species. This process was a key step in geopolymerization, wherein the dissolved Si and Al species re-polymerized into an aluminosilicate network.[27] Due to the higher structural stability and lower solubility of fly ash, its reaction with NaOH proceeded at a significantly slower rate compared to sodium silicate.[28] Overall, sodium silicate reacted almost immediately in NaOH, forming soluble silicate species, whereas fly ash underwent a slower dissolution and transformation process, primarily due to the presence of alumina and the greater strength of its Si–O–Si bonds.

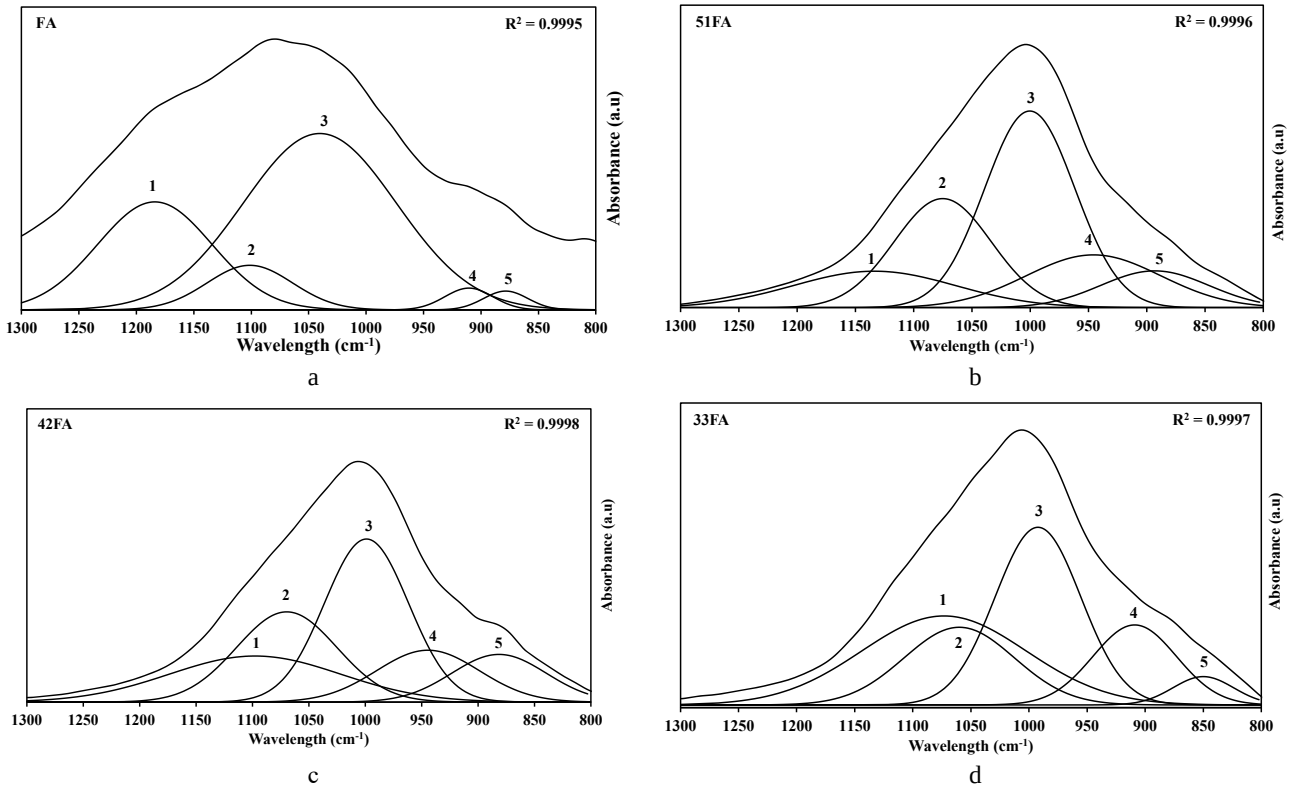

Fig. 5. Deconvolution of FT-IR spectra of FA a) and the prepared geopolymer b – d)

Therefore, after the washing process using distilled water, the loss of Si–O bonds in sodium silicate occurred. In addition, the percentage of Na^+ ions in the 42FA and 33FA samples was similar to that in the initial FA. Hence, the release of these Si^+ and Na^+ ions from the sodium silicate solution occurred. These results suggested that the suitable ratio in this study was 51FA, ensuring a balance of components during the geopolymerization process.

3.2.3. Porosity of the geopolymer

In the synthesis of geopolymers using high or sufficient concentrations of Na_2SiO_3 and NaOH, the resulting specific surface area, pore size, and pore volume were significantly influenced by the concentration and ratio of these alkaline activators. As illustrated in Fig. 6a, the geopolymers demonstrated a mesoporous structure consistent with Type IVa isotherms.[29] However, the amount of adsorbed nitrogen progressively declined with decreasing FA content in the synthesis composition. Additionally, the observed reduction in surface area might be attributed to the leaching of silicate and sodium species during the washing process. Silicate species were known to play a critical role in the formation of the geopolymer gel network in fly ash-based systems. The leaching of these species could disrupt the integrity of the gel structure, leading to a decrease in the amount of active material contributing to the surface area and resulting in a less porous microstructure.[30] Alkali activators, particularly sodium ions (Na^+), supported the maintenance of the charge balance and facilitated the polymerization process during geopolymer formation. The leaching of Na^+ ions could disrupt this charge equilibrium, thereby compromising the structural stability of the gel network. It was confirmed in Table 2 that the remained percentage of Na^+ ion was less in the 33FA sample than in the 51FA. Consequently, shrinkage or collapse of the pore walls might occur, leading to a reduction in the number and size of accessible pores.[31,32] For example, the Brunauer–Emmett–Teller (BET) surface area decreased from 99.8 m²/g for the 51FA to 89.7 m²/g for the 33FA sample. It has been reported that increasing the Na_2SiO_3/NaOH ratio led to the formation of a denser microstructure with reduced overall porosity.[33] Elevated sodium silicate content facilitated the formation of a more compact gel and accelerated the polycondensation process, thereby limiting the development of internal micro- and mesopores.[34] However, excessive Na_2SiO_3 concentrations might impede the geopolymerization process. This inhibition was attributed to the high concentration of Na^+ ions, which might hinder the interaction between reactive phases and precursor materials, resulting in incomplete reaction pathways and the entrapment of unreacted particles within a dense gel matrix, ultimately reducing porosity.[35,36] Pore size

was a critical microstructural parameter influenced by the type and concentration of activators, curing conditions, and the characteristics of the raw material. In the present study, a higher proportion of sodium silicate (alkali activator) in the geopolymer composition resulted in a decrease in the average pore size, with values of 4.2 nm for the 51FA and 3.8 nm for the 33FA sample. (Fig. 6b). Rapid gelation, induced by high activator concentrations, was able to encapsulate unreacted or partially reacted particles, leading to a decrease in accessible internal surfaces.[37] Furthermore, accelerated gel formation under high activator concentrations promoted a finer and more uniform pore structure. Consequently, the pore size distribution shifted toward smaller diameters, indicating that the formation of a denser gel phase under these conditions reduces the overall void volume.[38] A similar trend was observed in pore volume, which diminished as a result of rapid gelation and the formation of a denser structural network in the presence of elevated sodium silicate and sodium hydroxide contents. Excessive activator concentrations restricted the formation of larger capillary pores, thereby contributing to a lower total pore volume. Table 2 presents the porosity characteristics of the geopolymers synthesized with varying amounts of sodium silicate and alkali activator solution.

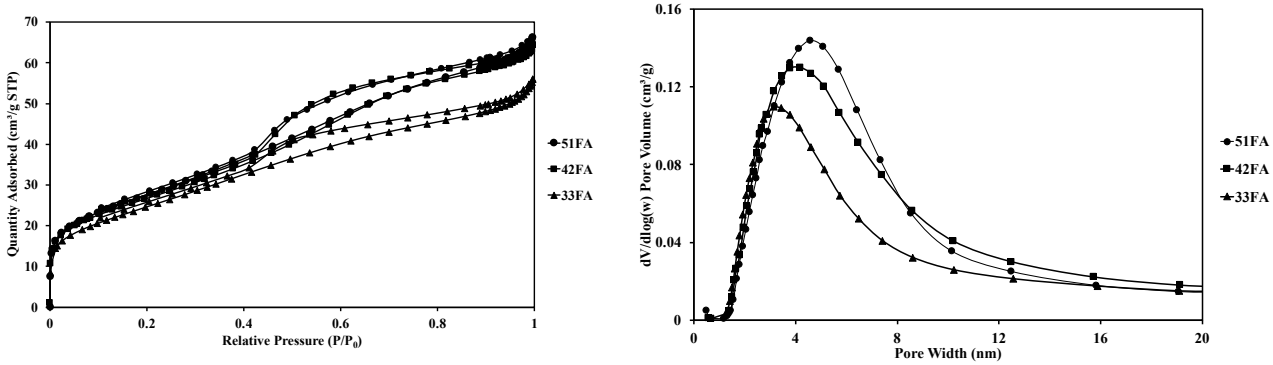

a b

Fig. 6. Nitrogen adsorption/desorption isotherms a) and the corresponding pore size distributions b) of the prepared geopolymer

3.2.4. pH_{pzc} of the geopolymer

The point of zero charge (pH_{pzc}) is a critical parameter that indicates the pH at which the surface of a material carries no net electrical charge. It directly influences the material's interaction with ionic species in solution, especially in applications such as adsorption, catalysis, or wastewater treatment. In this study, pH_{pzc} of the geopolymer synthesized from fly ash was determined to be approximately 8.0 **(**Fig. 7), similar to others.[39] This value remained relatively stable regardless of whether a high or sufficient amount of sodium silicate solution was used during synthesis. This observation suggested that the surface chemistry of the geopolymer was not significantly altered by increasing the sodium silicate content beyond a certain threshold. Sodium silicate acts as a source of soluble silica and also contributes to the alkaline environment necessary for geopolymerization. However, once the necessary amount of silicate was presented to facilitate the reaction and form a stable aluminosilicate gel network, further addition did not appear to influence the surface charge behavior, at least not to the extent that it shifted the pH_{pzc} value. The reason could be that the dominant surface functional groups, typically Si–OH and Al–OH groups, reach a saturation point in their chemical structure, beyond which extra silicate ions were either incorporated in a way that did not alter surface charge, or remained in the pore spaces or matrix without reacting. It also implied that the adsorptive behavior of the geopolymer would be relatively independent of moderate changes in the sodium silicate content.

3.3. Structural formulas

3.3.1. Effect of pH solution

The influence of pH on the adsorption behaviour of geopolymers is widely recognized as a critical parameter affecting their removal efficiency in aqueous environments. As illustrated in Fig. 8a, the removal efficiency of MB by the 51FA sample increased from 86.2% at pH 2 to 95.5% at pH 10, eventually reaching a plateau at approximately 99 % under highly alkaline conditions (pH 12). Similar trends were observed for the 42FA and 33FA samples, with maximum removal efficiencies also attained at pH 10. At low pH values, the high concentration of H^+ ions led to the protonation of the adsorbent surface, resulting in a net positive surface charge.

These protons competed with the cationic MB molecules for available adsorption sites, generating electrostatic repulsion that reduces the adsorption efficiency. Nevertheless, FA-based geopolymers were capable of

removing MB through ion-exchange mechanisms, whereby MB^+ cations replaced native alkali metal ions (*e.g.*, Na^+) within the geopolymer matrix. This ion exchange was enabled by the negatively charged aluminosilicate framework of the geopolymer, which maintained electroneutrality by accommodating exchangeable cations. Consequently, MB removal remained effective even at acidic pH levels (2 – 4).[40] Moreover, the porous structure of the geopolymer enhanced the ion-exchange and adsorption processes by offering abundant active sites, which was carried out in the porousity properties.[41] Under alkaline conditions, the presence of OH^- ions further induced a negatively charged adsorbent surface, which favors the electrostatic attraction of MB cations.

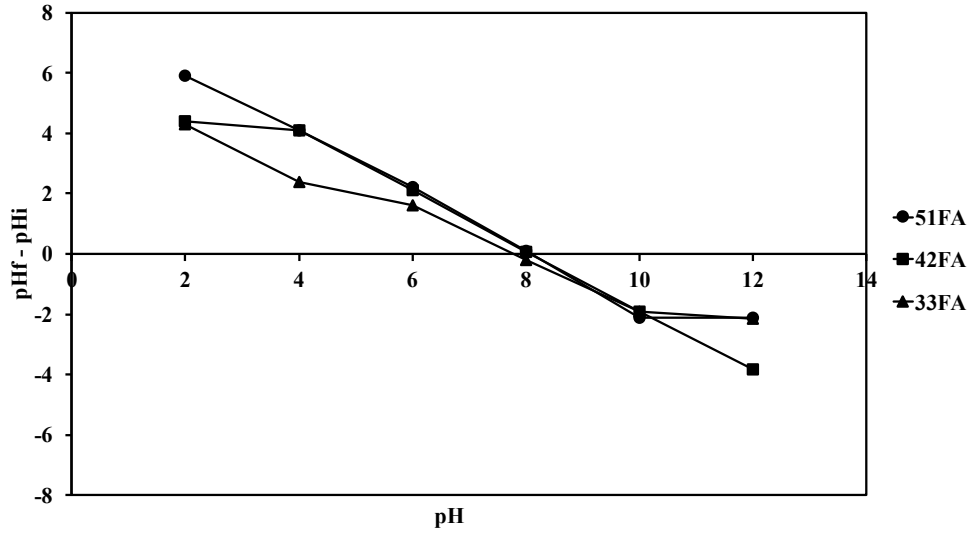

Fig. 7. pH_{pzc} of the prepared geopolymer

This suggested that electrostatic interactions between deprotonated hydroxyl groups (silanol groups) on the geopolymer surface and MB^+ were a primary driving force in the adsorption process. As shown in Fig. 8 b, the adsorption capacity of 51FA reached 18.3 mg/g at pH 8 and slightly increased to 18.5 and 18.8 mg/g at pH 10 and 12, respectively. Similarly, 42FA exhibited an increase from 17.8 to 18.5 mg/g, while 33FA increased from 17.7 to 18.1 mg/g over the same pH range. FT-IR spectral analysis indicated that the use of a higher concentration of alkali activators, such as Na_2SiO_3 and NaOH solution, during geopolymer synthesis might disrupt the formation of well-structured aluminosilicate linkages. This deficiency could result in fewer active adsorption sites, thereby reducing the material's overall MB uptake capacity. In this study, 51FA geopolymers were found to possess external silanol groups that readily deprotonate under alkaline conditions, contributing to their sustained adsorption performance. In addition, pH_{pzc} of geopolymers was obtained at 8, suggesting that the surface of geopolymers was able to be negative when dispersing in a solution having a pH higher than 8. Hence, the optimal MB removal was observed at pH 10, where the geopolymer surface exhibited the most favorable negative charge density for interacting with cationic MB molecules.

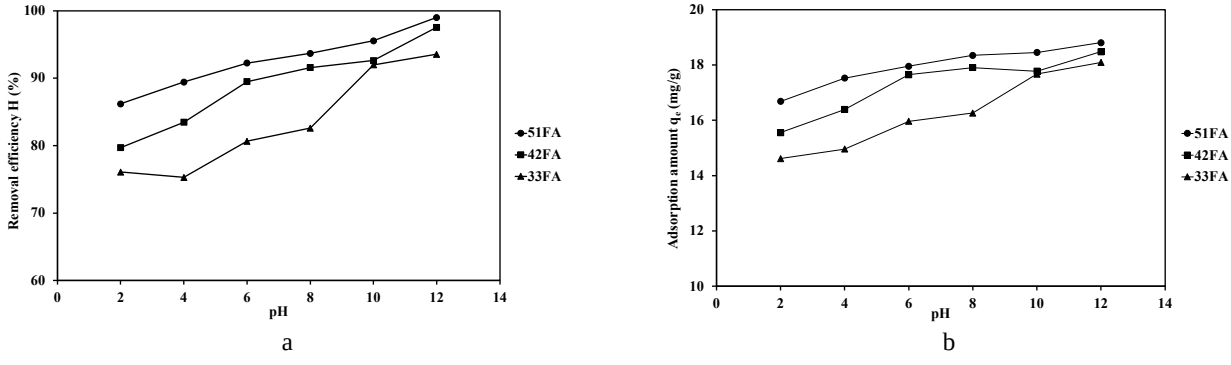

a b

Fig. 8. The removal efficiency a) and the adsorption amount b) of geopolymers to MB on the effect of pH

3.3.2. Effect of contact time

Similar to pH, contact time is another key parameter that significantly influences the adsorption performance of materials in water treatment applications. Determining the saturation capacity of an adsorbent over time is essential for optimizing its efficiency and operational feasibility. In this study, batch adsorption experiments were conducted using 0.1 g of adsorbent with an initial MB concentration of 100 mg/L at an optimized pH of 10. The contact time varied between 5 and 210 min to investigate its effect on MB removal. As shown in Fig. 9, the removal efficiency and adsorption capacity of the geopolymers generally increased with prolonged contact time. Notably, all samples exhibited a rapid initial uptake of MB, with more than 50% removal achieved within the first 5 min (Fig. 9a). For the 51FA sample, the removal efficiency increased progressively, reaching 91% at 120 min and peaking at 95.5% at 180 min, before slightly decreasing to 94.3% at 210 min. Similar trends were observed for the 42FA and 33FA samples as the removal efficiency for 42FA increased from 89.9% at 120 min to 92.6% at 180 min, while 33FA improved from 89.7% to 92.0% over the same time interval. However, further extension of the contact time to 210 min did not result in a significant improvement in MB removal, indicating that the equilibrium had been reached at 180 min. In addition, the adsorption capacity of the geopolymers for MB was found to improve with a lower loading of alkali activator solution, as shown in Fig. 9b. After 180 min of treatment, the adsorption capacity decreased from 18.6 mg/g for the 51FA to 17.9 mg/g for the 33FA sample. This trend indicated that a lower concentration of alkali activators during geopolymer synthesis might favor the development of more effective adsorption sites. These findings supported the notion that the majority of MB uptake occurred during the early stages of the adsorption process, likely due to the high availability of accessible surface active sites. As these sites became increasingly occupied over time, the rate of adsorption gradually declined, eventually reaching a state of dynamic equilibrium. This behavior was consistent with typical adsorption kinetics observed in porous materials. Here, the investigation of kinetic models was tested in terms of pseudo-first-order (PFO), pseudo-second-order (PSO), and intra-particle diffusion (IDP) models.

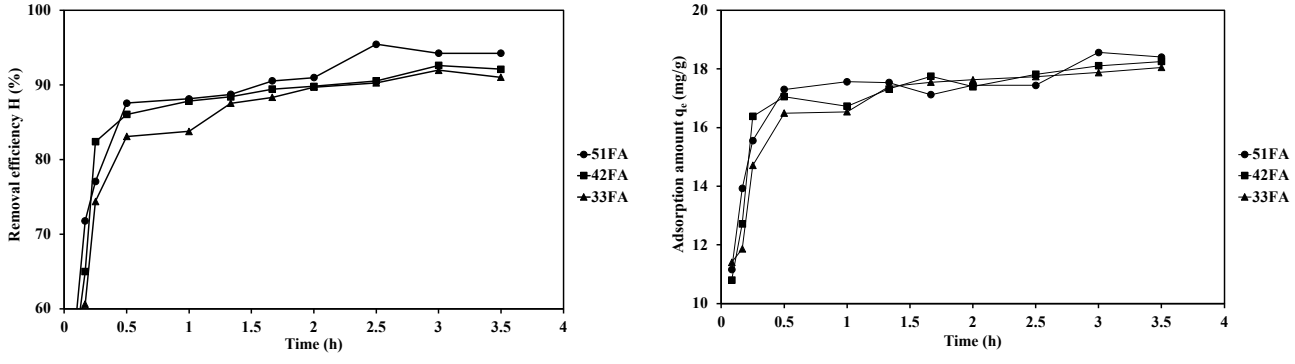

a b

Fig. 9. The removal efficiency a) and the adsorption amount b) of geopolymers to MB on the effect of contact time

The adsorption kinetics of MB onto the geopolymers were analyzed using PFO, PSO kinetic sand IPD models, as described by the following (Eqs. 3-5):[42,43]

$$Ln(q_e - q_t) = Lnq_e - k_1 t \quad (3)$$

$$\frac{1}{q_t} = \frac{1}{k_2 q_e^2} + \frac{t}{q_e} \quad (4)$$

$$q_t = kt^{1/2} + I \quad (5)$$

In these equations, q_e represents the amount of adsorbate adsorbed per unit mass of adsorbent at equilibrium (mg/g), while q_t is the amount adsorbed at a given time t (mg/g). k_1 denotes the rate constant of the PFO model (1/h), k_2 is the rate constant of the PSO model (g/mg·h), k is the intraparticle diffusion rate constant (mg/g·$h^{1/2}$), and I is a constant related to boundary layer thickness with diffusion resistance (mg/g).

Kinetic models were employed to elucidate the adsorption behaviour of geopolymers toward MB ions. As the contact time increased, the number of available active sites on the adsorbent surface gradually decreased, leading the system to approach adsorption equilibrium. The kinetic parameters are summarized in Table 3, with the

corresponding linear fittings presented in Figs. 10a and 10b. For all geopolymer samples, the correlation coefficients (R^2) for the PFO model were notably lower than those obtained for the PSO model, indicating a poorer fit. Specifically, for the 51FA sample, the R_2 value for the PFO model was 0.5371, which was significantly lower than the value obtained for the PSO model (0.9996). Furthermore, the equilibrium adsorption capacity (q_e) predicted by the PSO model (18.4 mg/g) closely aligned with the experimental value (18.6 mg/g), further validating the model's applicability. These findings suggested that the adsorption of MB onto geopolymers was more accurately described by the PSO model, implying that the process was primarily governed by chemisorption mechanisms. This involved surface complexation reactions, where cationic dye molecules interacted with negatively charged sites on the geopolymer surface through electron sharing or exchange. Moreover, the PSO rate constant (k_2) decreased from 1.6 to 0.8 g/mg·h for 51FA and 33FA, respectively, indicating a faster and more efficient chemisorption process in the 51FA sample. This behavior might be attributed to its higher surface area or more favourable pore structure, as confirmed by porosity measurements. Collectively, these results demonstrated that 51FA possessed superior surface characteristics, such as a greater number of reactive sites and stronger affinity for MB, which enhanced its adsorption performance under the studied conditions. To further investigate the influence of varying proportions of initial raw materials in the synthesis of geopolymers, the intraparticle diffusion model, commonly represented by the Weber–Morris (W–M) equation, was employed, as illustrated in Fig. 10c. Diffusion-based kinetic models typically describe adsorption as a multi-step process consisting of: (1) external mass transfer or film diffusion, which involves the transport of adsorbate molecules across the boundary layer surrounding the adsorbent particles; (2) intraparticle or pore diffusion, wherein the adsorbate migrates within the internal structure of the adsorbent through its pores or along pore walls; and (3) adsorption or desorption at active sites on the adsorbent surface, governed by mass action principles.[43]

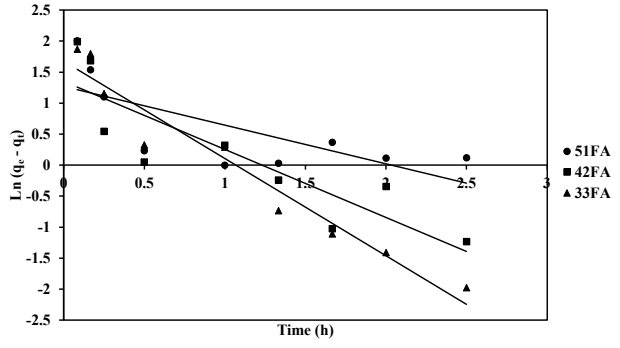

a

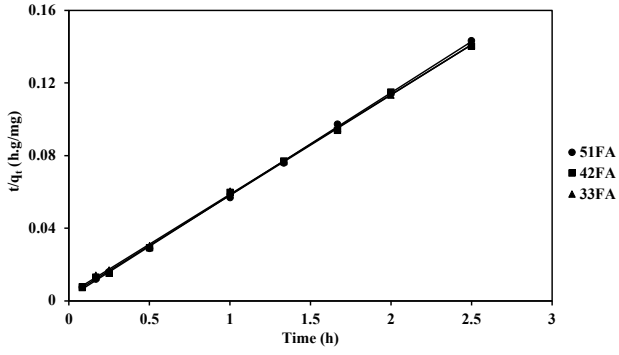

b

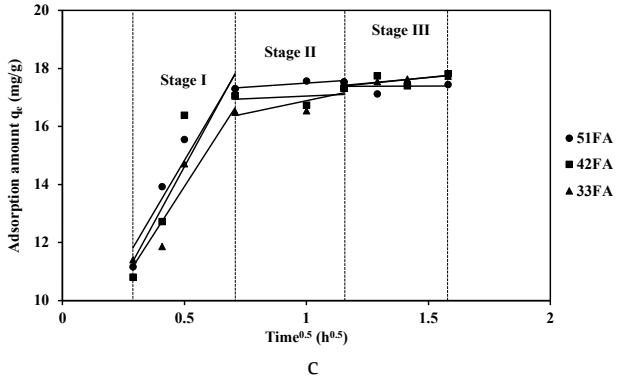

c

Fig. 10. Kinetic linear model of Pseudo-first-order a) and Pseudo-second-order b) and Intra-particle diffusion model c) of geopolymers

The adsorption performance of geopolymers synthesized from varying proportions of fly ash (FA) and an alkaline activator solution was further evaluated using the Weber–Morris (W–M) intra-particle diffusion (IDP) model. As illustrated in Fig. 10c, the adsorption process could be delineated into three distinct stages. In Stage I (initial adsorption phase), the rapid uptake of MB ions was primarily attributed to external surface adsorption, indicating that surface interaction mechanisms dominated at the early stage. The intraparticle diffusion rate constant k_1 increased with higher FA content in the geopolymer formulations (Table 3), suggesting improved initial

adsorption efficiency. Conversely, excessive incorporation of the Na_2SiO_3/NaOH activator solution may have contributed to a decrease in surface functional groups, thereby reducing the rate of adsorption at the external surface.[44] During Stage II (gradual adsorption phase), the diffusion of MB ions into the internal pores of the adsorbents became the rate-limiting step. A general decrease in the rate constant k_2 was observed across all geopolymer samples in this stage. Notably, the 51FA exhibited a relatively lower k_2 value (0.57 mg/g·$h^{1/2}$) than others, which could be attributed to its larger surface area.[45] Interestingly, 33FA showed an even higher k_2 value of 1.8 mg/g·$h^{1/2}$, implying that despite its comparatively lower porosity, the adsorption process was still efficient. This might be explained by the limited availability of internal pores, which promoted surface-dominated adsorption, thereby enhancing the apparent diffusion rate. Stage III (equilibrium phase) represented the final approach to saturation, where the adsorbate gradually diffused from mesopores into smaller micropores, leading to a significantly slower adsorption rate. The corresponding rate constant k_3 decreased with the reduction in the Na_2SiO_3/NaOH ratio, suggesting that lower alkaline content may hinder pore development, thereby limiting the accessibility of deeper adsorption sites.[46,47] These findings highlighted the complex interplay between pore structure, surface chemistry, and activator composition in governing the adsorption dynamics of FA-based geopolymers. Tailoring the ratio of precursor materials and alkaline solution was therefore critical to optimizing both surface and intraparticle adsorption mechanisms.[48]

Table 3. Kinetic parameters of PFO, PSO and IDP model of geopolymers to MB

Sample	Pseudo-first order (PFO)			Pseudo-second order (PSO)			Intraparticle diffusion (IDP)								
							Stage I			Stage II			Stage III		
	q_e (mg/g)	k_1 (1/h)	R^2	q_e (mg/g)	k_2 (g/mg.h)	R^2	k_1 (mg/g.$h^{1/2}$)	I_1 (mg/g)	R^2	k_2 (mg/g.$h^{1/2}$)	I_2 (mg/g)	R^2	k_3 (mg/g.$h^{1/2}$)	I_3 (mg/g)	R^2
51FA	3.6	0.62	0.5371	18.4	1.6	0.9996	0.57	16.9	0.8097	0.57	17.3	0.8021	0.028	16.9	0.8097
42FA	3.9	1.1	0.7674	18.1	1.1	0.9994	0.97	16.7	0.800	0.97	16.5	0.9797	0.79	16.7	0.800
33FA	5.4	1.6	0.9478	18.2	0.8	0.9996	1.8	15.2	0.6275	1.77	12.4	0.3916	0.085	15.2	0.6275

3.3.3. Effect of adsorbent dosage

The dosage of adsorbent played a pivotal role in determining the adsorption efficiency of FA-based geopolymers in water treatment applications. Increasing the adsorbent dosage generally enhanced the removal of contaminants due to the availability of more active binding sites. However, excessive dosages might lead to particle agglomeration and overlapping of adsorption sites, thereby reducing the adsorption capacity per unit mass. Consequently, optimizing the dosage was essential for balancing removal performance and material efficiency. In the case of geopolymers derived from fly ash, this optimization is influenced by factors such as precursor composition and the physicochemical characteristics imparted by the alkali activation process. In this study, the effect of adsorbent dosage on the removal of MB was investigated by varying the amount of geopolymer from 0.05 to 0.15 g in 20 mL of aqueous solution with an initial MB concentration of 100 mg/L at pH 10. After 180 min of treatment, both the removal efficiency and the adsorption capacity were evaluated. The corresponding results are presented in Fig. 11, illustrating the influence of geopolymer dosage on MB adsorption performance. Increasing the geopolymers improved the removal percentage of MB ions from water (Fig. 11a). For the 51FA sample, the removal efficiency of MB increased from 85.9% with 0.05 g of adsorbent to 95.5% with 0.1 g, and further reached 98.9% at 0.15 g. In contrast, samples with lower fly ash content as 42FA and 33FA, exhibited comparatively reduced removal efficiencies. Specifically, when the adsorbent dosage was raised from 0.05 to 0.1 g,

the removal efficiencies improved from 79.4% to 92.6% for 42FA and from 77.6% to 92.0% for 33FA. However, further increases in adsorbent dosage beyond 0.1 g did not result in substantial improvements, indicating the onset of adsorption saturation. Nonetheless, at higher dosages, the adsorption capacity per unit mass might decline due to particle aggregation, overlapping of adsorption sites, or reduced driving force for mass transfer at lower solute concentrations. This phenomenon was evident in the 51FA sample, where the adsorption capacity decreased from 18.5 mg/g at 0.1 g to 13.1 mg/g at 0.15 g. Similar trends were observed for 42FA and 33FA (Fig. 11b), suggesting a diminishing return in adsorption efficiency with excess dosage. Therefore, an optimal geopolymer dosage of 0.1 g was identified, balancing both high removal efficiency and effective material utilization.

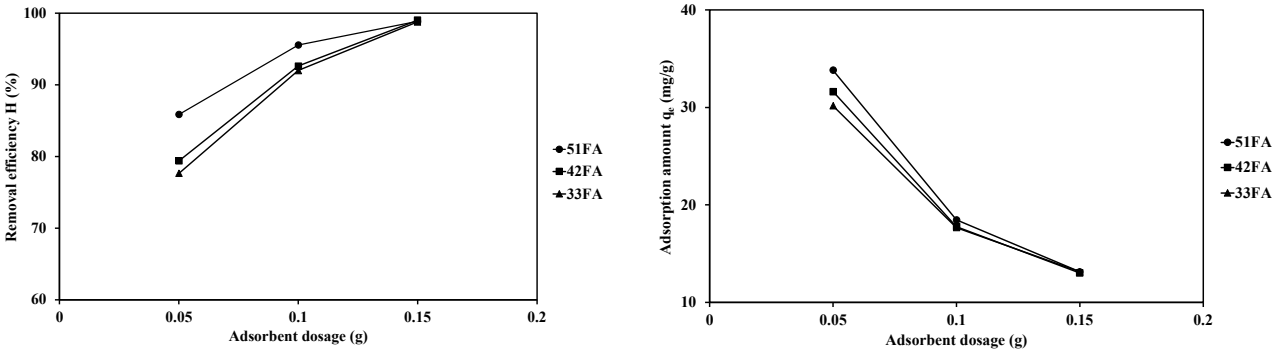

a b

Fig. 11. The removal efficiency a) and the adsorption amount b) of geopolymers to MB on the effect of adsorbent dosage

3.3.4. Effect of initial concentration

The initial concentration of MB plays a critical role in evaluating the efficiency of the adsorption process. The influence of initial MB concentration on the percentage removal by the geopolymer samples is illustrated in Fig. 12. As shown, all samples achieved nearly 100% removal efficiency when the initial MB concentration was 40 mg/L (Fig. 12a). Notably, even as the MB concentration increased from 60 to 100 mg/L, the removal efficiency of all samples remained above 90%. This trend could be attributed to the fact that higher MB concentrations might limit the availability of adsorption sites in the geopolymer matrix, thereby reducing removal efficiency. At lower initial concentrations, sufficient adsorption sites were available to accommodate MB ions effectively. A gradual decline in removal efficiency was observed with increasing Na_2SiO_3/NaOH ratios in the geopolymer compositions. This might be due to a reduction in the number of active adsorption sites associated with the FA content, as evidenced by the corresponding decreases in the surface area and pore size. At an initial MB concentration of 100 mg/L, the percentage removal was 91.9% for the 33FA sample and 95.3% for the 51FA sample. However, when the initial concentration increased to 120 mg/L, the removal efficiency declined to 81.8% and 74.8% for the 51FA and 33FA samples, respectively. As presented in Fig. 12 b, the initial concentration of MB significantly affected the adsorption performance of geopolymers with varying FA-to-alkaline activator ratios. The adsorption capacities remained relatively consistent across all samples when the MB concentration ranged from 40 to 100 mg/L.

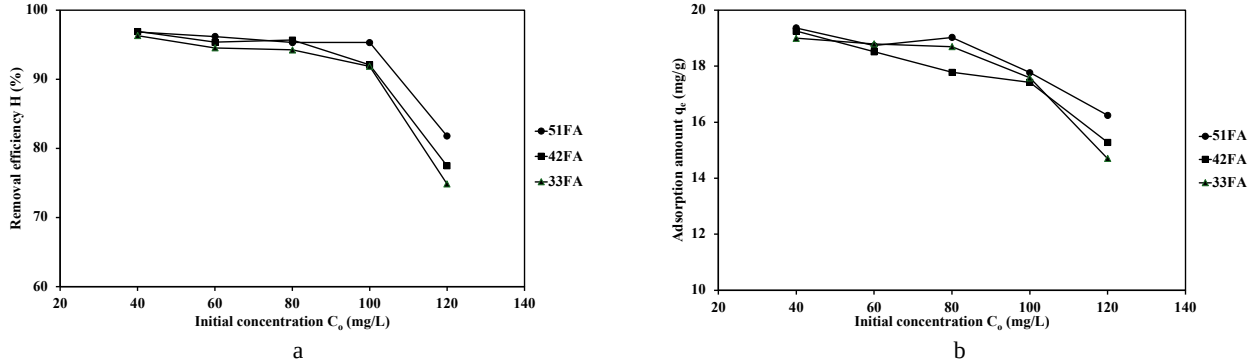

a b

Fig. 12. The removal efficiency a) and the adsorption amount b) of geopolymers to MB on the effect of initial concentration

However, at 120 mg/L, a slight reduction in uptake capacity was observed, corresponding to the FA content in the composites. These findings suggested that excessively high initial MB concentrations may exceed the capacity of available adsorption sites within the geopolymer structure, thereby limiting further adsorption.

Based on the previously established optimal pH and contact time, the effect of initial MB concentration on adsorption performance was further investigated. The adsorption behaviour of the FA-based geopolymers was analysed using both the Langmuir and the Freundlich isotherm models. These models were employed to elucidate the adsorption mechanism by evaluating the linear correlation coefficients (R^2) derived from their respective linearized equations. The Langmuir and the Freundlich isotherms were selected to describe the relationship between the equilibrium concentration of MB in the solution and the adsorption capacity of the geopolymers under constant temperature conditions. The linear form of the Langmuir isotherm model is expressed by the following (Eqs. 6 and 7):

$$\frac{C_e}{q_e} = \frac{1}{K_L q_m} + \frac{C_e}{q_m} \quad (6)$$

where q_m (mg/g) is the maximum adsorption capacity, and K_L (L.mg^{-1}) is the Langmuir constant.

The linear equation of the Freundlich isotherm model was presented as follows:

$$\ln q_e = \ln K_F + \frac{1}{n} \ln C_e \quad (7)$$

where K_F (L.g^{-1}) and n are the Freundlich isotherm constants related to the adsorption capacity and to the adsorption strength, respectively.

Isotherm modelling was conducted to evaluate the adsorption mechanism of FA-based geopolymers and to determine the relevant parameters of the Langmuir and the Freundlich models, based on their adsorption capacities at varying initial concentrations of MB. As shown by the linear plots in Fig. 13, the Langmuir isotherm model exhibited excellent agreement with the experimental data, with correlation coefficients (R^2) of 0.9992 for 33FA and 0.9997 for 51FA. In contrast, the Freundlich model produced lower R^2 values of 0.9647 for 33FA and 0.4704 for 51FA, indicating a less accurate fit, particularly for the latter one. These results strongly suggested that the Langmuir isotherm model more accurately described the adsorption process of MB onto FA-based geopolymers. The Langmuir model assumed monolayer adsorption on a surface with a finite number of identical and energetically equivalent adsorption sites. This indicated that MB molecules were likely adsorbed uniformly across the surface of the geopolymer, without interaction between adsorbed species. The excellent fit to the Langmuir model revealed a homogeneous distribution of active sites on the geopolymer surface, where each site binds a single MB molecule until saturation is reached. In contrast, the Freundlich isotherm model was an empirical model that described adsorption on heterogeneous surfaces and assumed that adsorption capacity varies with concentration. The lower R^2 values, particularly for 51FA, imply that this model did not adequately capture the behavior of MB adsorption on FA-based geopolymers, and that the adsorbent surface did not exhibit the level of heterogeneity assumed by the Freundlich model.[49] The parameters derived from the isotherm models are summarized in Table 4. Additionally, the maximum adsorption capacities (q_m) obtained from the Langmuir model were 18.7 mg/g for 51FA, 18 mg/g for 42FA, and 17.7 mg/g for 33FA indicating that higher fly ash content in the geopolymer correlates with increased adsorption capacity, likely due to the greater number of available active sites and improved surface characteristics favourable for dye adsorption.

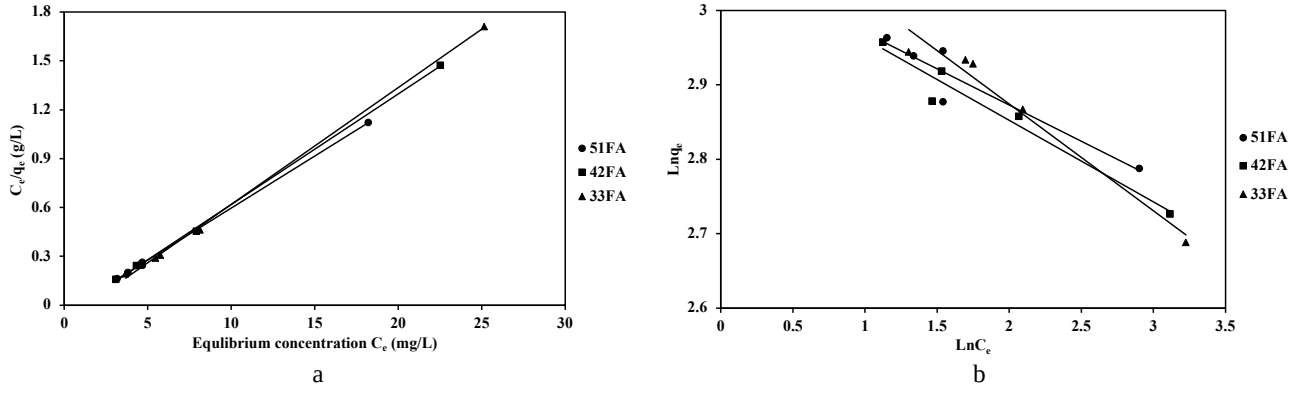

a b

Fig. 13. The Langmuir a) and the Freundlich b) linear adsorption isotherm of geopolymers to MB

Table 4. The adsorption isotherm parameters of MB by geopolymers

Sample	Langmuir			Freundlich		
	q_m (mg/g)	k_L ($L.g^{-1}$)	R^2	1/n	K_F ($L.g^{-1}$)	R^2
51FA	18.7	1.52	0.9997	0.097	21.5	0.8802
42FA	18.0	1.51	0.9982	0.086	19.9	0.4704
33FA	17.7	0.74	0.9992	0.143	23.6	0.9647

4. Conclusions

Various proportions of initial components were successfully employed in the synthesis of fly ash-based geopolymers. The resulting materials exhibited a decrease in porosity that correlated with lower FA content in the precursor mixture. This reduction in porosity was attributed to the formation of a denser gel structure, which limited the development of internal micro- and mesopores due to the higher content of alkaline activator (Na_2SiO_3/NaOH) in the system. The maximum adsorption capacity of MB cations decreased with increasing proportions of the Na_2SiO_3/NaOH mixture during synthesis. These findings emphasized the crucial role of the initial mixing ratios of raw materials and alkaline activators in determining the structural characteristics of the geopolymers, which in turn significantly influenced their adsorption performance in dye removal applications. Building on the findings of this study, future research could explore the balance between surface adsorption and pore-filling mechanisms, providing new insights into designing geopolymers with targeted adsorption capacities for specific pollutants. Interestingly, variations in the proportion of alkaline activator in the geopolymer composition influenced the maximum adsorption capacity of MB cation, which was recorded as 18.7 mg/g for 51FA, 18.0 mg/g for 41FA, and 17.8 mg/g for 33FA. Additionally, the recyclability and long-term stability of FA-based geopolymers in continuous flow systems remain important areas for further investigation, especially for large-scale wastewater treatment applications. Moreover, extending this approach to other industrial wastes could promote the development of hybrid geopolymer adsorbents with improved structural and functional properties. Ultimately, this research supports the broader pursuit of sustainable materials in environmental remediation and underscores the value of industrial by-products as resources in circular economy strategies.

References

[1] Pham, N. Q.; Le, K. A. Coal Fly Ash in Vietnam and its Application as a Lightweight Material. *Chem. Eng. Trans.* **2021**, *83*, 31–36. https://doi.org/10.3303/CET2183006

[2] Mathapati, M.; Amate, K.; Durga Prasad, C.; Jayavardhana, M. L.; Hemanth Raju, T. A Review on Fly Ash Utilization. *Mater. Today Proc.* **2022**, *50*, 1535–1540. https://doi.org/10.1016/j.matpr.2021.09.106

[3] Li, H.; Xu, D. The Future Resources for eco-Building Materials: II. Fly ash And Coal Waste. *J. Wuhan Univ. Technol.-Mat. Sci. Edit.* **2009**, *24*, 667–672. http://doi.org/10.1007/s11595-009-4667-7

[4] Rao, Z.; Yu, W.; Yuan, H.; Wei, P.; Yang, F.; Nyarko-Appiah, J. E. Eco-Friendly and Efficient Alumina Recovery from Coal Fly Ash by Employing the CaO as an Additive During the Vacuum Carbothermic Reduction and Alkali Dissolution. *J. Sustain. Metall.* **2024**, 10, 2216–2226 http://doi.org/10.1007/s40831-024-00916-0

[5] Davidovits, J. Geopolymers: Inorganic Polymeric New Materials. *J. Therm. Anal. Calorim.* **1991**, *37*, 1633–1656. http://doi.org/10.1007/BF01912193

[6] Onutai, S.; Kobayashi, T.; Thavorniti, P.; Jiemsirilers, S. Porous Fly Ash-Based Geopolymer Composite Fiber as an Adsorbent for Removal of Heavy Metal Ions from Wastewater. *Mater. Lett.* **2019**, *236*, 30–33. https://doi.org/10.1016/j.matlet.2018.10.035

[7] Onutai, S.; Jiemsirilers, S.; Thavorniti, P.; Kobayashi, T. Aluminium Hydroxide Waste Based Geopolymer Composed of Fly Ash for Sustainable Cement Materials. *Constr. Build. Mater.* **2015**, *101*, 298–308. https://doi.org/10.1016/j.conbuildmat.2015.10.097

[8] Novais, R. M.; Carvalheiras, J.; Tobaldi, D. M.; Seabra, M. P.; Pullar, R. C.; Labrincha, J. A. Synthesis of Porous Biomass Fly Ash-Based Geopolymer Spheres for Efficient Removal of Methylene Blue from Wastewaters. *J. Clean. Prod.* **2019**, *207*, 350–362. https://doi.org/10.1016/j.jclepro.2018.09.265

[9] Maleki, A.; Mohammad, M.; Emdadi, Z.; Asim, N.; Azizi, M.; Safaei, J. Adsorbent Materials Based on a Geopolymer Paste for Dye Removal from Aqueous Solutions. *Arab. J. Chem.* **2020**, *13*, 3017–3025. https://doi.org/10.1016/j.arabjc.2018.08.011

[10] Onutai, S. In *Development of geopolymer materials sourced with fly ash and industrial waste*, 2016.

[11] Pimraksa, K.; Chindaprasirt, P.; Rungchet, A.; Sagoe-Crentsil, K.; Sato, T. Lightweight Geopolymer Made of Highly Porous Siliceous Materials with Various Na_2O/Al_2O_3 and SiO_2/Al_2O_3 Ratios. *Mater. Sci. Eng. A* **2011**, *528*, 6616–6623. https://doi.org/10.1016/j.msea.2011.04.044

[12] Nguyen, K. D.; Tran, A. T. H.; Kaus, N. H. M. Preparation and Characterization of Red Mud-Based Geopolymer Composited with Rice Husk Ash for the Adsorption of Bromocresol Green in Aqueous Solution. *Chem. Chem. Technol.* **2023**, *17*, 857–869. https://doi.org/10.23939/chcht17.04.857

[13] Yao, X.; Zhang, Z.; Zhu, H.; Chen, Y. Geopolymerization Process of Alkali–Metakaolinite Characterized by Isothermal Calorimetry. *Thermochimica Acta* **2009**, *493*, 49–54. https://doi.org/10.1016/j.tca.2009.04.002

[14] Sasui, S.; Kim, G.; van Riessen, A.; Lim, C.; Eu, H.; Park, J.; Nam, J. Effects of Na_2SiO_3/NaOH Ratio in Alkali Activator on the Microstructure, Strength and Chloride Ingress in fly Ash and

GGBS Based Alkali Activated Concrete. *J. Build. Eng.* **2024**, *98*, 111255. https://doi.org/10.1016/j.jobe.2024.111255
[15] Salleh, M. A. M.; Mahmoud, D. K.; Karim, W. A.; Idris, A. Cationic and Anionic Dye Adsorption By Agricultural Solid Wastes: A Comprehensive Review. *Desalination* **2011**, *280*, 1-13. https://doi.org/10.1016/j.desal.2011.07.019
[16] Ma, G.; Zhu, Y.; Zhang, Z.; Li, L. Preparation and Characterization of Multi-Walled Carbon Nanotube/TiO_2 Composites: Decontamination Organic Pollutant in Water. *Appl. Surf. Sci.* **2014**, *313*, 817–822. https://doi.org/10.1016/j.apsusc.2014.06.079
[17] Chen, Q.; He, Q.; Lv, M.; Xu, Y.; Yang, H.; Liu, X.; Wei, F. Selective Adsorption of Cationic Dyes by UiO-66-NH_2. *Appl. Surf. Sci.* **2015**, *327*, 77–85. https://doi.org/10.1016/j.apsusc.2014.11.103
[18] Takele, T.; Angassa, K.; Abewaa, M.; Kebede, A. M.; Tessema, I. Adsorption of Methylene Blue from Textile Industrial Wastewater Using Activated Carbon Developed from H_3PO_4-Activated Khat Stem Waste. *Biomass Convers. Biorefin.* **2025**, *15*, 4085–4108. http://doi.org/10.1007/s13399-023-05245-y
[19] el Alouani, M.; Alehyen, S.; el Achouri, M.; Taibi, M. H. Removal of Cationic Dye - Methylene Blue- from Aqueous Solution by Adsorption on Fly Ash-Based Geopolymer. *J. Mater. Environ. Sci.* **2018**, *9*, 32–46. http://doi.org/10.26872/jmes.2018.9.1.5
[20] Modi, S.; Yadav, V. K.; Gacem, A.; Ali, I. H.; Dave, D.; Khan, S. H.; Yadav, K. K.; Rather, S.-u.; Ahn, Y.; Son, C. T.; *et al*. Recent and Emerging Trends in Remediation of Methylene Blue Dye from Wastewater by Using Zinc Oxide Nanoparticles. *Water* **2022**, *14*, 1749. http://doi.org/10.3390/w14111749
[21] Yang, Y.; Le, T.-C.-D.; Kudo, I.; Do, T.-M.-D.; Niihara, K.; Suematsu, H.; Thorogood, G. Pore-Forming Process in Dehydration of Metakaolin-Based Geopolymer. *International Journal of Ceramic Engineering & Science* **2021**, *30*, 211–216. https://doi.org/10.1002/ces2.10100
[22] Sulistiyo, Y. A.; Andriana, N.; Piluharto, B.; Zulfikar, Z. Silica Gels from Coal Fly Ash as Methylene Blue Adsorbent: Isotherm and Kinetic Studies. *Bull. Chem. React. Eng. Catal.* **2017**, *12*, 10. http://doi.org/10.9767/bcrec.12.2.766.263-272
[23] Sinha, D. K.; Kumar, A.; K.; Kumar, S. Development of Geopolymer Concrete from Fly Ash and Bottom Ash Mixture. *Trans. Indian Ceram. Soc.* **2014**, *73*, 143–148. https://doi.org/10.1080/0371750X.2014.922427
[24] Petrus, H. T.; Olvianas, M.; Shafiyurrahman, M. F.; Pratama, I. G.; Jenie, S. N.; Astuti, W.; Nurpratama, M. I.; Ekaputri, J. J.; Anggara, F. Circular Economy of Coal Fly Ash and Silica Geothermal for Green Geopolymer: Characteristic and Kinetic Study. *Gels* **2022**, *8*, 233 http://doi.org/10.3390/gels8040233
[25] Dupuis, R.; Pellenq, R.; Champenois, J.-B.; Poulesquen, A. Dissociation Mechanisms of Dissolved Alkali Silicates in Sodium Hydroxide. *J. Phys. Chem. C.* **2020**, *124*, 8288–8294. http://doi.org/10.1021/acs.jpcc.0c01495
[26] Matinfar, M.; Nychka, J. A. A review of Sodium Silicate Solutions: Structure, Gelation, and Syneresis. *Adv. Colloid Interface Sci.* **2023**, *322*, 103036. https://doi.org/10.1016/j.cis.2023.103036
[27] Adewuyi, Y. G. Recent Advances in Fly-Ash-Based Geopolymers: Potential on the Utilization for Sustainable Environmental Remediation. *ACS Omega* **2021**, *6*, 15532–15542. http://doi.org/10.1021/acsomega.1c00662
[28] Luhar, I.; Luhar, S. A Comprehensive Review on Fly Ash-Based Geopolymer. *J. Compos. Sci.* **2022**, *6*, 219 http://doi.org/10.3390/jcs6080219
[29] Rahman, M. M.; Muttakin, M.; Pal, A.; Shafiullah, A. Z.; Saha, B. B. A Statistical Approach to Determine Optimal Models for IUPAC-Classified Adsorption Isotherms. *Energies* **2019**, *12*, 4565 http://doi.org/10.3390/en12234565
[30] Rattanasak, U.; Chindaprasirt, P. Influence of NaOH solution on the synthesis of fly ash geopolymer. *Miner. Eng.* **2009**, *22*, 1073–1078. https://doi.org/10.1016/j.mineng.2009.03.022
[31] Guerrieri, M.; Sanjayan, J.; Mohd Ali, A. Z. Geopolymer damage due to leaching when exposed to water. In *Concrete Durability and Service Life Planning*; Kovler, K.; Zhutovsky, S.; Spatari, S.; Jensen, O. M., Eds.; Springer International Publishing, Cham, 2020; pp 74–78.
[32] Lv, X.-s.; Qin, Y.; Lin, Z.-x.; Tian, Z.-k.; Cui, X.-m. Inhibition of Efflorescence in Na-Based Geopolymer Inorganic Coating. *ACS Omega* **2020**, *5*, 14822–14830. http://doi.org/10.1021/acsomega.0c01919
[33] Morsy, M. S.; Alsayed, S. H.; Al-Salloum, Y.; Almusallam, T. Effect of Sodium Silicate to Sodium Hydroxide Ratios on Strength and Microstructure of Fly Ash Geopolymer Binder. *Arab. J. Sci. Eng.* **2014**, *39*, 4333–4339. http://doi.org/10.1007/s13369-014-1093-8
[34] Matinfar, M.; Nychka, J. A. Process Mapping of the Sol–Gel Transition in Acid-Initiated Sodium Silicate Solutions. *Gels* **2024**, *10*, 673 http://doi.org/10.3390/gels10100673
[35] Kwek, S. Y.; Awang, H.; Cheah, C. B. Influence of Liquid-to-Solid and Alkaline Activator (Sodium Silicate to Sodium Hydroxide) Ratios on Fresh and Hardened Properties of Alkali-Activated Palm Oil Fuel Ash Geopolymer *Materials* **2021**, *14*, 4253. https://doi.org/10.3390/ma14154253
[36] Efe, M.; Öz, A.; Bayrak, B.; Kaplan, G.; Aydın, A. C. Effect of Na_2SiO_3/NaOH Rate and Natural Zeolite Content on Basalt Fiber Reinforced Eco-Efficient Slag-Based Geopolymer Mortar Synthesis. *Arch. Civ. Mech. Eng.* **2024**, *24*, 215. http://doi.org/10.1007/s43452-024-01021-5
[37] Katoueizadeh, E.; Rasouli, M.; Zebarjad, S. M. A Comprehensive Study on the Gelation Process of Silica Gels from Sodium Silicate. *J. Mater. Res. Technol.* **2020**, *9*, 10157–10165. https://doi.org/10.1016/j.jmrt.2020.07.020
[38] Kugbe, J.; Matsue, N.; Henmi, T. Synthesis of Linde Type A zeolite–Goethite Nanocomposite as an Adsorbent for Cationic and Anionic Pollutants. *J. Hazard. Mater.* **2009**, *164*, 929–935. https://doi.org/10.1016/j.jhazmat.2008.08.080
[39] Nguyen, K. D.; My, Q. N. V.; Kim, A. P. T.; Tran, P. T.; Huynh, D. T. K.; Le, O. T. K. Coal Fly Ash-Slag and Slag-Based Geopolymer as an Absorbent for the Removal of Methylene Blue in Wastewater. *STDJ* **2022**, *25*, 2215–2223. https://doi.org/10.32508/stdj.v25i1.3421
[40] Rivera-Muñoz, E. M.; Nava, R.; Velázquez-Castillo, R.; Manzano-Ramírez, A.; Ramón, J.; Apátiga-Castro, M.; Rodríguez-López, A. Ion Exchange in Geopolymers. In *New Trends in Ion Exchange Studies*, Karakuş, S., Ed.; IntechOpen: Rijeka, 2018. http://doi.org/10.5772/intechopen.80970
[41] Li, C. J.; Zhang, Y. J.; Chen, H.; He, P. Y.; Meng, Q. Development of Porous and Reusable Geopolymer Adsorbents for Dye Wastewater Treatment. *J. Clean. Prod.* **2022**, *348*, 131278. https://doi.org/10.1016/j.jclepro.2022.131278
[42] El Alouani, M.; Alehyen, S.; El Achouri, M.; Taibi, M. h. Adsorption of Cationic Dye onto Fly Ash-Based Geopolymer:

Batch and Fixed Bed Column Studies. *MATEC Web Conf.* **2018**, *149*, 02088.
[43] Hasani, N.; Selimi, T.; Mele, A.; Thaçi, V.; Halili, J.; Berisha, A.;Sadiku, M. Theoretical, Equilibrium, Kinetics and Thermodynamic Investigations of Methylene Blue Adsorption onto Lignite Coal. *Molecules* **2022**, *27*, 1856. https://doi.org/10.3390/molecules27061856
[44] Heah, C. Y.; Kamarudin, H.; Bakri, A. M. M. A.; Binhussain, M.; Luqman, M.; Nizar, I. K.; Ruzaidi, C. M.; Liew, Y. M. Effect of Curing Profile on Kaolin-based Geopolymers. *Phys. Procedia* **2011**, *22*, 305–311. https://doi.org/10.1016/j.phpro.2011.11.048
[45] Komnitsas, K.; Zaharaki, D. Geopolymerisation: A Review and Prospects for the Minerals Industry. *Miner. Eng.* **2007**, *20*, 1261–1277. https://doi.org/10.1016/j.mineng.2007.07.011
[46] Singh, B.; Ishwarya, G.; Gupta, M.; Bhattacharyya, S. K. Geopolymer Concrete: A Review of Some Recent Developments. *Constr. Build. Mater.* **2015**, *85*, 78–90. https://doi.org/10.1016/j.conbuildmat.2015.03.036
[47] Temuujin, J.; Minjigmaa, A.; Lee, M.; Chen-Tan, N.; van Riessen, A. Characterisation of Class F fly Ash Geopolymer Pastes Immersed in Acid and Alkaline Solutions. *Cem. Concr. Compos.* **2011**, *33*, 1086–1091. https://doi.org/10.1016/j.cemconcomp.2011.08.008
[48] Bakharev, T. Geopolymeric materials prepared using Class F fly ash and elevated temperature curing. *Cem. Concr. Res.* **2005**, *35*, 1224–1232. https://doi.org/10.1016/j.cemconres.2004.06.031
[49] Zhou, Y.; Zhang, M.; Hu, X.; Wang, X.; Niu, J.; Ma, T. Adsorption of Cationic Dyes on a Cellulose-Based Multicarboxyl Adsorbent. *J. Chem. Eng. Data* **2013**, *58*, 413–421. http://doi.org/10.1021/je301140c

Received: April 28, 2025 / Revised: September 03, 2025 / Accepted: September 05, 2025

СТІЙКА ВАЛОРИЗАЦІЯ ЗОЛИ В АДСОРБЕНТ НА ОСНОВІ ГЕОПОЛІМЕРУ: ОПТИМІЗАЦІЯ СТРУКТУРИ ТА ЕФЕКТИВНІСТЬ ВИДАЛЕННЯ МЕТИЛЕНУ-СИНЬОГО

Анотація. *У цьому дослідженні геополімери на основі золи (FA) були синтезовані з використанням різних пропорцій розчину силікату натрію/гідроксиду натрію (Na_2SiO_3/ NaOH 10M), від 49% у зразку 51FA до 67% у зразку 33FA, які використовувалися для адсорбції метиленового синього (MB) у воді. Після затвердіння при 60 °C протягом 24 годин пористість отриманих геополімерів зменшилася, що було пов'язано з посиленням процесу поліконденсації, спричиненим збільшенням вмісту Na_2SiO_3, що призвело до утворення більш компактної гелевої структури в отриманому геополімері. Модель Вебера-Морріса показала, що поверхневі взаємодії з молекулами MB були переважними в зразку 51FA, тоді як механізми заповнення пор були більш вираженими в геополімері 33FA. Експерименти з адсорбції показали, що всі зразки геополімерів відповідали ізотермічній моделі Ленгмюра, з коефіцієнтами кореляції, що наближалися до одиниці.*

Ключові слова: *лужний активатор, в'яжучий матеріал, геополімер, зола, регенеровані відходи.*